J Mol Model (2013) 19:3119–3125
DOI 10.1007/s00894-013-1847-3

ORIGINAL PAPER

# Structural transitions in mixed ternary noble gas clusters

**Xia Wu · Yan Sun · Yin-Chun Gao · Gen-Hua Wu**

Received: 11 December 2012 / Accepted: 2 April 2013 / Published online: 23 April 2013


**Abstract** The properties of noble gas systems can be greatly extended by heterogeneous mixtures of elements. The geometrical structures and energies of mixed Ar–Kr–Xe clusters were investigated using ternary Lennard-Jones (TLJ) potential. For the $Ar_{19}Kr_nXe_{19}$, $Ar_{19}Kr_{19}Xe_n$, and $Ar_nKr_{19}Xe_{19}$ ($n$=0–17) clusters investigated, the results show that only two minimum energy configurations exist, i.e., polytetrahedron and six-fold pancake. The inner core of all these clusters is composed mainly of Ar atoms, and Kr and Xe atoms are distributed on the surface with well mixed pattern for polytetrahedral and segregate pattern for six-fold pancake configurations. The relative stability property of Ar–Kr–Xe clusters with a certain composition is discussed. Moreover, the role of heterogeneity on the strain was investigated, and reduced strain energies in Ar–Kr–Xe clusters were studied to find possible ways of reducing strain. The results showed that the strain energies were affected mainly by Ar–Ar, Ar–Kr, and Xe–Xe bonds.

**Keywords** Noble gas · Ar–Kr–Xe cluster · Lennard-Jones potential · Structural optimization

## Introduction

Atomic / molecular clusters containing from a few to tens of thousands of atoms have been much studied because of their unique, size-dependent structures and properties that differ from the bulk chemical [1]. Many studies have traced the structural growth patterns of atomic clusters of different sizes to study their properties. Experimental and theoretical studies implied that the structure of noble gas clusters is icosahedral at small size and undergoes a direct transition to being face centered cubic (fcc) with increasing size [2–4]. Clusters of argon, krypton, and xenon are grown in a free jet and ionized by electron impact, and pronounced "magic numbers" in the distributions of large cluster ions occur at sizes of 147 (148 for Ar), 309, and 561 [5]. Formation of the electronic band structure by the valence-shell of Ar, Kr, and Xe clusters was studied for various cluster sizes using angle-resolved photoelectron spectroscopy [6]. Furthermore, various theoretical calculations were applied to noble gas clusters and dimers to study their interatomic interaction [7–12]. For example, potential energy curves for three homonuclear ($He_2$, $Ne_2$, $Ar_2$) and three heteronuclear (He–Ne, He–Ar, Ne–Ar) rare gas dimers were calculated using several correlation consistent basis sets and the supermolecule single and double excitation coupled-cluster theory with noniterative perturbational treatment of triple excitations [7]. The intermolecular potentials for the helium and argon dimer have been computed using infinite-order symmetry-adapted perturbation theory and very large orbital and explicitly correlated basis sets [8, 9].

As a model for noble gas clusters, Lennard-Jones (LJ) potential has been investigated widely, including homogeneous LJ clusters, binary LJ clusters [13, 14], ternary LJ (TLJ) [15] clusters, and even quinary $Ar_{11}Kr_{11}Xe_{11}He_{11}Ne_{11}$ clusters [16]. For instance, Marques and Pereira use LJ potential and improved LJ potentials to describe pair interactions in $Ar_nKr_{38-n}$, $Ar_nXe_{38-n}$, and $Kr_nXe_{38-n}$ clusters [17]. On the other hand, LJ potential is also used as a benchmark system for testing the efficiency of global optimization algorithms. For instance, at the early time, by lattice searching, the efficiency of the genetic algorithm (GA) was improved for optimization of LJ clusters up to 147 atoms [18]. Later, investigation on icosahedral lattices was accomplished up to 309-atom LJ clusters [19]. In the work of Shao et al., LJ

X. Wu (✉) · Y.-C. Gao · G.-H. Wu
School of Chemistry and Chemical Engineering, Anqing Normal University, Anqing 246011, People's Republic of China
e-mail: xiawu@aqtc.edu.cn

Y. Sun
College of Chemical Engineering, Hebei United University, Tangshan 063009, People's Republic of China

clusters in the size range of 310–561 were located for the first time also by GA and lattice construction [20]. For the optimization of $LJ_{561-1610}$ clusters, lattice searching was performed using a greedy search method [21]. On the other hand, LJ potential is also used in other areas, e.g., the interaction carbon in single-walled carbon nanotubes (SWNTs) and the surrounding fluid [22].

Global optimization of binary clusters is a challenging problem in computational chemistry. The potential energy surface of binary clusters is much more complicated than that of monatomic clusters. Besides geometrical isomers in optimization of monoatomic clusters, homotopic isomers with a fixed number of atoms, the same composition and geometry, but different ordering patterns of the atoms must also be considered, thus both continuous and combinatorial optimization have to be solved. Optimization algorithms, such as GA [16, 23], the basin-hopping Monte Carlo algorithm [24, 25], and adaptive immune optimization algorithm (AIOA) [15, 26, 27] have been developed for the optimization of binary clusters. Recently, the efficiency of the big-bang method for the optimization of atomic clusters was analyzed in detail for Morse pair potentials with different parameters ranges [28]. For geometry optimization of bimetallic clusters, Lai et al. [29] proposed an efficient heuristic algorithm composed of three ingredients: a monotonic basin-hopping method with guided perturbation (MBH-GP), a surface optimization method, and an iterated local search (ILS) method, where MBH-GP and surface optimization method are used to optimize the geometric structure of a cluster, and the ILS method is used to search the optimal homotop for a fixed geometric structure. Similarly, another heuristic algorithm (denoted by 3OP) that makes extensive use of three perturbation operators was proposed for binary LJ clusters [30]. In our previous studies, AIOA was applied successfully to the structural optimization of ternary clusters such as TLJ clusters and Cu–Ag–Au clusters [15, 27].

In this study, the geometrical structures and energies of mixed $Ar_{19}Kr_nXe_{19}$, $Ar_{19}Kr_{19}Xe_n$, and $Ar_nKr_{19}Xe_{19}$ ($n$=0–17) clusters were investigated, and TLJ potential was applied to study the structural transition in Ar–Kr–Xe clusters. Then, reduced strain energies for Ar–Ar, Kr–Kr, Xe–Xe, Ar–Kr, Ar–Xe, and Kr–Xe interactions were analyzed to propose possible ways of reducing strain.

## Methods

### Ternary Lennard-Jones potential

The interatomic interaction of Ar–Kr–Xe clusters is described by TLJ potential [15]. LJ potential is a pairwise potential comprising a long-range attractive part and a short-range repulsive part, which has been intensively investigated. The potential is given by

$$E = 4\varepsilon_{ij}\sum_{1\le i<j\le N}\left[\left(\frac{\sigma_{ij}}{r_{ij}}\right)^{12}-\left(\frac{\sigma_{ij}}{r_{ij}}\right)^{6}\right] = \varepsilon_{ij}\sum_{1\le i<j\le N}\left[\left(\frac{1}{x_{ij}}\right)^{12}-2\left(\frac{1}{x_{ij}}\right)^{6}\right] \quad (1)$$

where $N$ is the number of atoms, and $r_{ij}$ represents the distance between atoms $i$ and $j$; $\varepsilon_{ij}$ is the pair well depth, and $\sigma_{ij}$ is cluster diameter (size). In Ar–Kr–Xe clusters, with respect to argon ($\sigma_{ArAr}$=1.00, $\varepsilon_{ArAr}$=1.00), the present datum for $\sigma$ and $\varepsilon$ are thus $\sigma_{KrKr}$=1.12403, $\sigma_{XeXe}$=1.206, $\sigma_{ArKr}$=1.062, $\sigma_{KrXe}$=1.16397, $\sigma_{ArXe}$=1.074, $\varepsilon_{KrKr}$=1.373534, $\varepsilon_{XeXe}$=1.852, $\varepsilon_{ArKr}$=1.1717, $\varepsilon_{KrXe}$=1.59914, and $\varepsilon_{ArXe}$=1.48. The parameters are taken from references [31] and [32]. The potential energy of a stable Ar–Kr–Xe cluster is calculated according to Eq. (1), and the lowest value of potential energy corresponds to the minimum energy structure.

### Adaptive immune optimization algorithm

The minimum energy structures of ternary Ar–Kr–Xe clusters are optimized by using AIOA [26, 27]. AIOA is an adaptive heuristic search algorithm based on the evolutionary ideas of natural genetic selection and clonal selection principles, which takes the basic frame of GA. The basic steps of the AIOA include an immune clone selection and a mutation operation. First, a number of configurations are generated randomly and optimized locally, and these configurations form an original gene library. Then, a population of individuals is selected from the gene library by a selection probability in the immune clone selection procedure described in [26]. Subsequently, the mutation operation is performed on the selected individuals to generate new individuals. For binary and ternary clusters, in the mutation of a generation (a repetition), 50 % of individuals are selected with energy-based mutation for geometrical isomers, and the other 50 % of individuals are selected by an atom exchange operation, i.e., two type atoms are selected randomly and their location is exchanged for the homotopic isomers in binary or ternary clusters. The lower energy individual is kept in the library for the updating operation. Finally, the combination of selection, mutation, and updating operations is repeated until a preset maximal iteration number is reached. Therefore, application of AIOA can find the stable structure of a ternary cluster. In this study, 200 independent runs were performed, and minimum energy structures appear at least twice.

## Results and discussion

### Stable structures of Ar–Kr–Xe clusters

Putative stable structures of $Ar_{19}Kr_nXe_{19}$ ($n$=0–17), $Ar_{19}Kr_{19}Xe_n$ ($n$=0–17), and $Ar_nKr_{19}Xe_{19}$ ($n$=0–17) clusters were investigated by AIOA. The investigated size starts from 38 (i.e., $n$=0) because it may have an especially stable fcc structure [33]. Moreover, the geometries of stoichiometric (19:19) clusters have been studied widely, and represent a well mixed pattern of the first and the second rare gas atoms [27]. These 54 optimized structures are shown in Figs. 1, 2 and 3, respectively, and their potential energies calculated from Eq. (1) are listed in Table 1 for reference. From these figures, it is clear that, in all clusters, only two types, i.e., polytetrahedron [34] and six-fold pancake, of the minimum energy configurations can be found. The polytetrahedral configuration is found in aluminum clusters with glue [35] and binary LJ [13] potential, and can also explain the structure of quasicrystals and atomic liquids and glasses. The six-fold pancake configuration is found in Ag-Au [36] and Ag-Pd clusters [37] with Gupta potentials.

At first, in $Ar_{19}Kr_nXe_{19}$ ($n$=0–17) clusters as shown in Fig. 1, $Ar_{19}Xe_{19}$ has a polytetrahedral structure with most Ar atoms in the inner-shell and Xe atoms on the surface, and the distribution of Ar and Xe atoms is similar to that discussed in [31]. With the increase in size $n$ from 1 to 14, it can be seen that all clusters have polytetrahedral structures. In $Ar_{19}Kr_nXe_{19}$ ($n$=1–14) clusters, the inner core is occupied mostly by Ar atoms, and Xe atoms are distributed on the surface as in the $Ar_{19}Xe_{19}$ cluster. Furthermore, the added Kr atoms are dispersed on the surface, and Kr and Xe atoms are mixed on the surface. However, at $Ar_{19}Kr_nXe_{19}$ ($n$=15–17) clusters, the motif becomes six-fold pancake. Specifically, the central atom of these clusters is Xe, surrounded by 12 Ar atoms. These Ar atoms are then further surrounded by Kr and Xe atoms, but Kr and Xe atoms are significantly segregated. Kr atoms tend to be together around the inner core, and Xe atoms are located on the top and bottom sites.

For $Ar_{19}Kr_{19}Xe_n$ ($n$=0–17) clusters in Fig. 2, with the increasing $n$ from 0 to 12, it is clear that all clusters have polytetrahedral structures. In these clusters, the inner core is occupied mostly by Ar atoms, and Kr atoms are distributed on the surface. Furthermore, the added Xe atoms are dispersed on the surface, and Kr and Xe atoms are mixed on the surface. However, for $Ar_{19}Kr_{19}Xe_n$ ($n$=13–17) clusters, the motif is a six-fold pancake. Specifically, the central atom of these clusters is Xe, surrounded by 12 Ar atoms as in $Ar_{19}Kr_{19}Xe_n$ ($n$=13–17) clusters, with Ar atoms further surrounded by Kr and Xe atoms. Moreover, Kr and Xe atoms are significantly segregated.

In Fig. 3, for $Ar_nKr_{19}Xe_{19}$ ($n$=0–17) clusters, upon increasing $n$ from 0 to 14, it can be seen that all clusters have

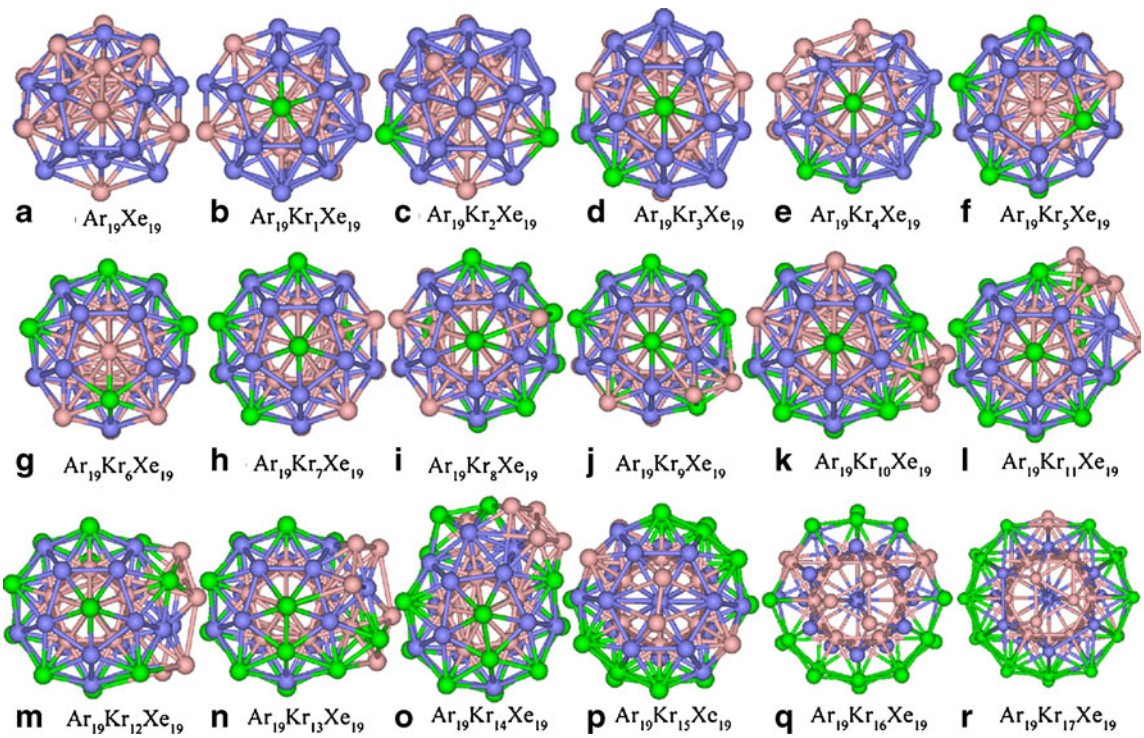


**Fig. 1** Putative global minimal structures of $Ar_{19}Kr_nXe_{19}$ ($n$=0–17) clusters, and Ar, Kr, and Xe atoms are represented by *pink*, *green*, and *blue spheres*, respectively

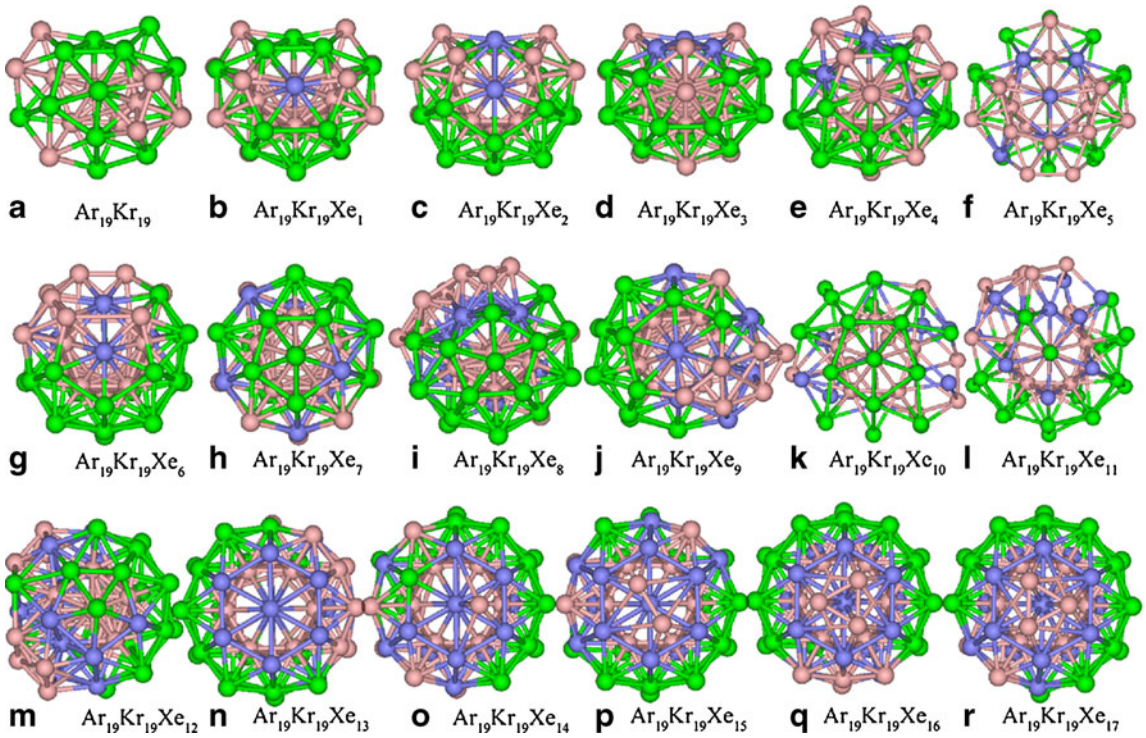


**Fig. 2** Putative global minimal structures of $Ar_{19}Kr_{19}Xe_n$ ($n$=0–17) clusters, and Ar, Kr, and Xe atoms are represented by *pink*, *green*, and *blue spheres*, respectively

polytetrahedral structures. In the $Kr_{19}Xe_{19}$ cluster, the inner two sites are occupied by Kr atoms, and mixed Kr and Xe atoms occupy the other sites. It can be deduced that icosahedral Kr–Xe clusters prefer to have Kr atoms at the center, which is contrary to the argument that atoms with larger $\varepsilon$ prefer to occupy interior sites [31]. Furthermore,

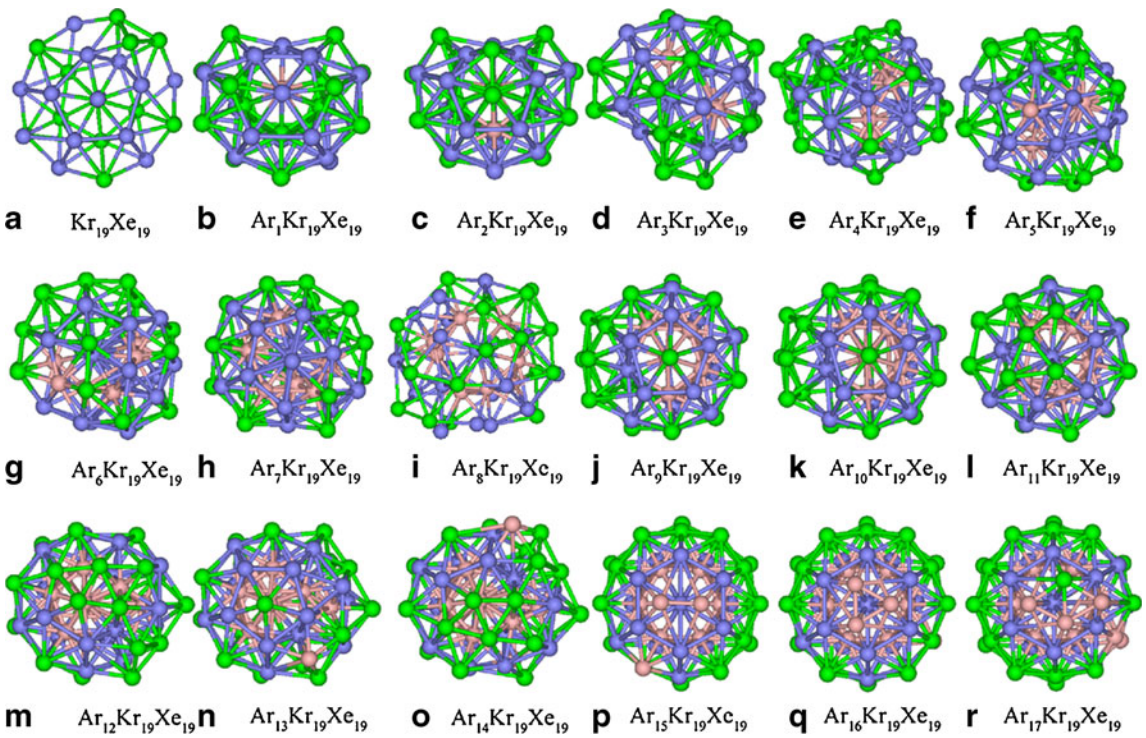


**Fig. 3** Putative global minimal structures of $Ar_nKr_{19}Xe_{19}$ ($n$=0–17) clusters, and Ar, Kr, and Xe atoms are represented by *pink*, *green*, and *blue spheres*, respectively

**Table 1** Calculated potential energies (eV) by Eq. (1) of the lowest-energy structures of $Ar_{19}Kr_nXe_{19}$, $Ar_{19}Kr_{19}Xe_n$, and $Ar_nKr_{19}Xe_{19}$ ($n$=0–17) clusters by adaptive immune optimization algorithm (AIOA)

| Composition | Energy | Composition | Energy | Composition | Energy |
|---|---|---|---|---|---|
| $Ar_{19}Xe_{19}$ | −264.9268 | $Ar_{19}Kr_{19}$ | −214.3887 | $Kr_{19}Xe_{19}$ | −284.9237 |
| $Ar_{19}Kr_1Xe_{19}$ | −274.3766 | $Ar_{19}Kr_{19}Xe_1$ | −225.8778 | $Ar_1Kr_{19}Xe_{19}$ | −293.4400 |
| $Ar_{19}Kr_2Xe_{19}$ | −281.8266 | $Ar_{19}Kr_{19}Xe_2$ | −236.3539 | $Ar_2Kr_{19}Xe_{19}$ | −300.3948 |
| $Ar_{19}Kr_3Xe_{19}$ | −291.0287 | $Ar_{19}Kr_{19}Xe_3$ | −247.3493 | $Ar_3Kr_{19}Xe_{19}$ | −307.6664 |
| $Ar_{19}Kr_4Xe_{19}$ | −299.3599 | $Ar_{19}Kr_{19}Xe_4$ | −258.6374 | $Ar_4Kr_{19}Xe_{19}$ | −315.5574 |
| $Ar_{19}Kr_5Xe_{19}$ | −308.9872 | $Ar_{19}Kr_{19}Xe_5$ | −269.3847 | $Ar_5Kr_{19}Xe_{19}$ | −322.6130 |
| $Ar_{19}Kr_6Xe_{19}$ | −318.8992 | $Ar_{19}Kr_{19}Xe_6$ | −280.8627 | $Ar_6Kr_{19}Xe_{19}$ | −330.6011 |
| $Ar_{19}Kr_7Xe_{19}$ | −328.9015 | $Ar_{19}Kr_{19}Xe_7$ | −291.6813 | $Ar_7Kr_{19}Xe_{19}$ | −337.6220 |
| $Ar_{19}Kr_8Xe_{19}$ | −336.1134 | $Ar_{19}Kr_{19}Xe_8$ | −302.9095 | $Ar_8Kr_{19}Xe_{19}$ | −346.1141 |
| $Ar_{19}Kr_9Xe_{19}$ | −343.9866 | $Ar_{19}Kr_{19}Xe_9$ | −313.8974 | $Ar_9Kr_{19}Xe_{19}$ | −353.1805 |
| $Ar_{19}Kr_{10}Xe_{19}$ | −352.6397 | $Ar_{19}Kr_{19}Xe_{10}$ | −325.3386 | $Ar_{10}Kr_{19}Xe_{19}$ | −361.2532 |
| $Ar_{19}Kr_{11}Xe_{19}$ | −360.2104 | $Ar_{19}Kr_{19}Xe_{11}$ | −336.2299 | $Ar_{11}Kr_{19}Xe_{19}$ | −368.6469 |
| $Ar_{19}Kr_{12}Xe_{19}$ | −368.5227 | $Ar_{19}Kr_{19}Xe_{12}$ | −348.1803 | $Ar_{12}Kr_{19}Xe_{19}$ | −375.9860 |
| $Ar_{19}Kr_{13}Xe_{19}$ | −376.6796 | $Ar_{19}Kr_{19}Xe_{13}$ | −359.8349 | $Ar_{13}Kr_{19}Xe_{19}$ | −383.6541 |
| $Ar_{19}Kr_{14}Xe_{19}$ | −384.5583 | $Ar_{19}Kr_{19}Xe_{14}$ | −370.1720 | $Ar_{14}Kr_{19}Xe_{19}$ | −389.8877 |
| $Ar_{19}Kr_{15}Xe_{19}$ | −392.7321 | $Ar_{19}Kr_{19}Xe_{15}$ | −381.7628 | $Ar_{15}Kr_{19}Xe_{19}$ | −397.7976 |
| $Ar_{19}Kr_{16}Xe_{19}$ | −401.6754 | $Ar_{19}Kr_{19}Xe_{16}$ | −393.7416 | $Ar_{16}Kr_{19}Xe_{19}$ | −405.3291 |
| $Ar_{19}Kr_{17}Xe_{19}$ | −409.2088 | $Ar_{19}Kr_{19}Xe_{17}$ | −404.1559 | $Ar_{17}Kr_{19}Xe_{19}$ | −411.5283 |

from the figure, it is clear that the added Ar atoms grow mainly in the inner core, and Kr and Xe atoms on the surface have a similar growth pattern as in Figs. 1 and 2. Moreover, for $Ar_nKr_{19}Xe_{19}$ ($n$=15–17) clusters, the motif is a six-fold pancake. Specifically, the location of the central Xe atom and surface atoms of Kr and Xe is similar to the case in $Ar_{19}Kr_nXe_{19}$ ($n$=15–17) and $Ar_{19}Kr_{19}Xe_n$ ($n$=13–17) clusters. Clearly, Ar–Kr–Xe clusters tend to be polytetrahedral structures with sizes smaller than 53, and six-fold pancake structures with sizes of 53–55.

From Figs. 1, 2 and 3, it can be seen that, in these clusters, when $n$ is smaller than 13, i.e., the atomic number of one element is smaller than those of other two elements, Ar–Kr–Xe clusters adopt the polytetrahedron motif. However, when $n \geq 13$, i.e., the atomic number of Ar, Kr, and Xe is close, a six-fold pancake is formed easily with similar atomic distribution of the Ar, Kr, and Xe in clusters.

## Energy analysis of Ar–Kr–Xe clusters

To analyze the stability of a cluster of a certain composition compared to its neighbors, the second order finite difference $\Delta_2 E$ is applied. For instance, in $Ar_{19}Kr_nXe_{19}$ clusters, $\Delta_2 E$ is the energy released by migrating one Kr atom from $Ar_{19}Kr_{n+1}Xe_{19}$ to $Ar_{19}Kr_{n-1}Xe_{19}$ to form two $Ar_{19}Kr_nXe_{19}$ particles, and it is defined as $\Delta_2 E = E_{\min}(N+1) + E_{\min}(N-1) - 2E_{\min}(N)$ of the energy, where $E_{\min}(N)$ is the potential energy of minimum structure for $N$-atom Ar–Kr–Xe clusters. Figure 4 plots $\Delta_2 E$ for $Ar_{19}Kr_nXe_{19}$, $Ar_{19}Kr_{19}Xe_n$, and $Ar_nKr_{19}Xe_{19}$ ($n$=0–17) clusters with size $n$. In the figure, the positive peaks of $\Delta_2 E$ correspond to particularly stable structures with respect to their neighbors, which are usually designated as magic numbers observed in mass spectra. From the curves of $Ar_{19}Kr_nXe_{19}$ and $Ar_{19}Kr_{19}Xe_n$ ($n$=0–17) clusters, peaks are almost the same at $n$=4, 6, 8, 10, and 13. Furthermore, from the results of the second difference three apparent positive peaks, i.e., $Ar_3Kr_{19}Xe_{19}$, $Ar_7Kr_{19}Xe_{19}$, and $Ar_{10}Kr_{19}Xe_{19}$, are found in $Ar_nKr_{19}Xe_{19}$ ($n$=0–17) clusters. However, we could not check this hypothesis because of the scarcity of reports on the energies or structures of their lowest-energy clusters.

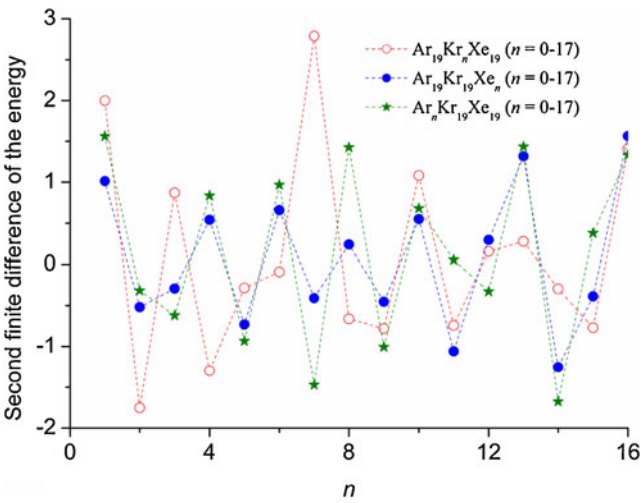


**Fig. 4** Second finite differences of the energies of the optimized $Ar_{19}Kr_nXe_{19}$ ($n$=0–17), $Ar_{19}Kr_{19}Xe_n$ ($n$=0–17), and $Ar_nKr_{19}Xe_{19}$ ($n$=0–17) clusters

Reduced strain energies in Ar–Kr–Xe clusters

The role of heterogeneity on the strain in Ar–Kr–Xe clusters was investigated, and the various contributions to the reduced strain energies, i.e., the strain energy divided by both the corresponding number of nearest neighbors and the pair potential well depth [31], were computed. The strain energies for Ar–Ar, Kr–Kr, Xe–Xe, Ar–Kr, Ar–Xe, and Kr–Xe interactions are defined as follows [33]:

$$E^{\text{strain}}_{\text{Ar-Ar}} = E_{\text{Ar-Ar}} + N^{nn}_{\text{Ar-Ar}}\varepsilon_{\text{Ar-Ar}} \quad (2)$$

$$E^{\text{strain}}_{\text{Kr-Kr}} = E_{\text{Kr-Kr}} + N^{nn}_{\text{Kr-Kr}}\varepsilon_{\text{Kr-Kr}} \quad (3)$$

$$E^{\text{strain}}_{\text{Xe-Xe}} = E_{\text{Xe-Xe}} + N^{nn}_{\text{Xe-Xe}}\varepsilon_{\text{Xe-Xe}} \quad (4)$$

$$E^{\text{strain}}_{\text{Ar-Kr}} = E_{\text{Ar-Kr}} + N^{nn}_{\text{Ar-Kr}}\varepsilon_{\text{Ar-Kr}} \quad (5)$$

$$E^{\text{strain}}_{\text{Ar-Xe}} = E_{\text{Ar-Xe}} + N^{nn}_{\text{Ar-Xe}}\varepsilon_{\text{Ar-Xe}} \quad (6)$$

$$E^{\text{strain}}_{\text{Kr-Xe}} = E_{\text{Kr-Xe}} + N^{nn}_{\text{Kr-Xe}}\varepsilon_{\text{Kr-Xe}} \quad (7)$$

In these equations, $E_{\text{X-Y}}$ is the total binding energy between atoms X and Y, $N^{nn}_{\text{X-Y}}$ is the number of X−Y nearest neighbors, which is given by $N^{nn}_{\text{X-Y}} = \sum_{i<j}\delta_{ij}$, if $r_{ij} \leq 1.2\sigma_{ij}$ , $\delta_{ij}=1$, otherwise, $\delta_{ij}=0$. Lennard-Jones well depth $\varepsilon$X-Y corresponds to the interaction between X and Y atoms. Reduced strain energies are defined as $e^{\text{strain}} = E^{\text{strain}}/N^{nn}\varepsilon$ to account for the different magnitudes of the interactions among atom types. In term of these definitions, the strain energies are always positive quantities. The strain energies of $Ar_{19}Kr_nXe_{19}$, $Ar_{19}Kr_{19}Xe_n$, and $Ar_nKr_{19}Xe_{19}$ ($n$=0–17) clusters are represented versus composition in Fig. 5. They give us some insight into possible ways of reducing strain.

From Fig. 5a, it seems to be clear that, in $Ar_{19}Kr_nXe_{19}$ ($n$=0–17) clusters, the total strain energies of all bonds for six-fold pancake structures are lowest at $n$=15–17. However, for $n$=0–14, polytetrahedral structures have relatively high strain energies. This can be accounted for by high Ar–Ar and Ar–Kr strain energies in the figure. In $Ar_{19}Kr_{19}Xe_n$ ($n$=0–17) clusters of Fig. 5b, the strain energies are determined mainly by Ar–Ar and Xe–Xe bonds, and for six-fold pancake structures at $n$=13–17, their values are relatively low. Furthermore, in the area of high strain energies, i.e., $n$=1–2, the Kr–Kr bonds generate a high strain energy. Moreover, the strain energies of polytetrahedral clusters, i.e., $n$=0–14, are higher than those of six-fold pancake clusters at $n$=15–17. Therefore, it can be seen that Ar–Ar, Ar–Kr, and Xe–Xe bonds affect the strain energies.

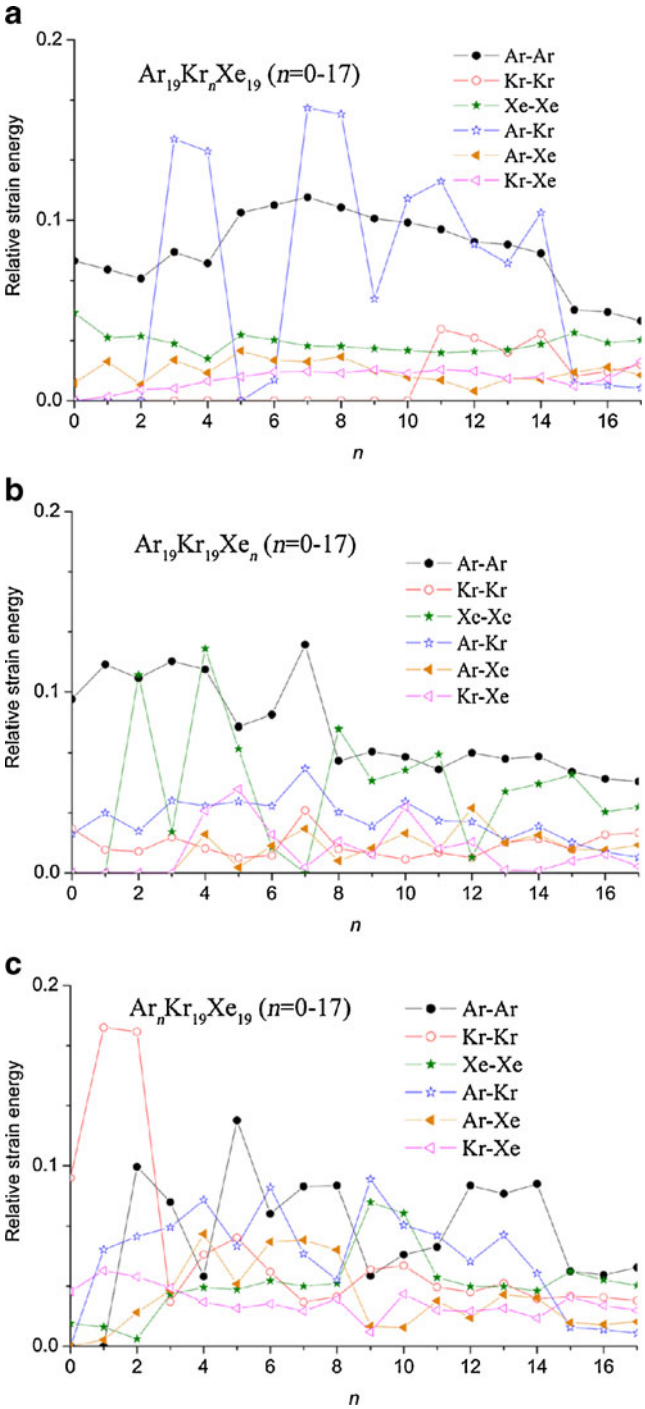


**Fig. 5** Reduced strain energies for Ar–Ar, Kr–Kr, Xe–Xe, Ar–Kr, Ar–Xe, and Kr–Xe interactions in **a** $Ar_{19}Kr_nXe_{19}$ ($n$=0–17) clusters, **b** $Ar_{19}Kr_{19}Xe_n$ ($n$=0–17), and **c** $Ar_nKr_{19}Xe_{19}$ ($n$=0–17) clusters

## Conclusions

The geometrical structures and energies of mixed Ar–Kr–Xe clusters were investigated by AIOA. Mixed $Ar_{19}Kr_nXe_{19}$, $Ar_{19}Kr_{19}Xe_n$, and $Ar_nKr_{19}Xe_{19}$ ($n$=0–17) clusters were

optimized. The results show that only two minimum energy configurations exist, i.e., polytetrahedron and six-fold pancake. The inner core of all these clusters is composed mainly of Ar atoms, and Kr and Xe atoms are distributed on the surface, with a well mixed pattern for polytetrahedral and segregative pattern for six-fold pancake configurations. Reduced strain energies for Ar–Ar, Kr–Kr, Xe–Xe, Ar–Kr, Ar–Xe, and Kr–Xe interactions were then analyzed to propose possible ways of reducing strain. The results show that Ar–Ar, Ar–Kr, and Xe–Xe bonds affect strain energies. This finding might be helpful for the theoretical guidance and experimental validation of Ar–Kr–Xe clusters. From the analysis of strain energies, it could be concluded that Ar–Kr–Xe clusters with six-fold pancake structures might be the most stable, and this is expected to be validated experimentally.

**Acknowledgments** This study was supported by National Natural Science Foundation of China (NNSFC) (Nos. 21203002 and 21171008) and Anhui Provincial Natural Science Foundation (No. 1308085QB29). The authors thank X.G. Shao for a Grant from the Adaptive Immune Optimization Algorithm (AIOA) program from Nankai University.

## References

1. Castleman AW Jr, Keesee RG (1988) Gas-phase clusters: spanning the states of matter. Science 241:36–42
2. Bordner AJ (2012) Assessing the accuracy of SAPT(DFT) interaction energies by comparison with experimentally derived noble gas potentials and molecular crystal lattice energies. ChemPhysChem 13:3981–3988
3. Lee JW, Stein GD (1987) Structure change with size of argon clusters formed in laval nozzle beams. J Phys Chem 91:2450–2457
4. Zweiback J, Ditmire T, Perry MD (1999) Femtosecond time-resolved studies of the dynamics of noble-gas cluster explosions. Phys Rev A 59:3166–3169
5. Miehle W, Kandler O, Leisner T, Echt O (1989) Mass spectrometric evidence for icosahedral structure in large rare gas clusters: Ar, Kr, Xe. J Chem Phys 91:5940–5952
6. Rolles D, Zhanga H, Pešić ZD, Bozek JD, Berrah N (2009) Emergence of valence band structure in rare-gas clusters. Chem Phys Lett 468:148–152
7. Cybulski SM, Toczyłowski RR (1999) Ground state potential energy curves for $He_2$, $Ne_2$, $Ar_2$, He–Ne, He–Ar, and Ne–Ar: a coupled-cluster study. J Chem Phys 111:10520–10528
8. Jeziorska M, Cencek W, Patkowski K, Jeziorski B, Szalewicz K (2007) Pair potential for helium from symmetry-adapted perturbation theory calculations and from supermolecular data. J Chem Phys 127:124303
9. Williams HL, Korona T, Bukowski R, Jeziorski B, Szalewicz K (1996) Helium dimer potential from symmetry-adapted perturbation theory. Chem Phys Lett 262:431–436
10. Patkowski K, Szalewicz K (2010) Argon pair potential at basis set and excitation limits. J Chem Phys 133:094304
11. Pillardy J, Olszewski KA, Piela L (1992) Performance of the shift method of global minimization in searches for optimum structures of clusters of Lennard-Jones atoms. J Phys Chem 96:4337–4341
12. Hermann A, Schwerdtfeger P (2009) Complete basis set limit second-order Møller-Plesset calculations for the fcc lattices of neon, argon, krypton, and xenon. J Chem Phys 131:244508
13. Doye JPK, Meyer L (2005) Mapping the magic numbers in binary Lennard-Jones clusters. Phys Rev Lett 95:063401
14. de Souza VK, Wales DJ (2009) Connectivity in the potential energy landscape for binary Lennard-Jones systems. J Chem Phys 130:194508
15. Wu X, Sun Y, Li CS, Yang W (2012) Parametric effects of the potential energy function on the geometrical features of ternary Lennard-Jones clusters. J Phys Chem A 116:8218–8225
16. Dieterich JM, Hartke B (2011) Composition-induced structural transitions in mixed Lennard-Jones clusters: global reparametrization and optimization. J Comput Chem 32:1377–1385
17. Marques JMC, Pereira FB (2013) A detailed investigation on the global minimum structures of mixed rare-gas clusters: geometry, energetics, and site occupancy. J Comput Chem 34:505–517. doi:10.1002/jcc.23161
18. Northby JA (1987) Structure and binding of Lennard-Jones clusters: $13 \le N \le 147$. J Chem Phys 87:6166–6177
19. Romero D, Barron C, Gomez S (1999) The optimal geometry of Lennard-Jones clusters: 148–309. Comput Phys Commun 123:87–96
20. Xiang YH, Jiang HY, Cai WS, Shao XG (2004) An efficient method based on lattice construction and the genetic algorithm for optimization of large Lennard-Jones clusters. J Phys Chem A 108:3586–3592
21. Xiang YH, Cheng LJ, Cai WS, Shao XG (2004) Structural distribution of Lennard-Jones clusters containing 562 to 1000 atoms. J Phys Chem A 108:9516–9520
22. Hu M, Shenogin S, Keblinski P (2007) Thermal energy exchange between carbon nanotube and air. Appl Phys Lett 90:231905
23. Johnston RL (2003) Evolving better nanoparticles: genetic algorithms for optimising cluster geometries. J Chem Soc Dalton Trans 22:4193–4207
24. Hsu PJ, Lai SK (2006) Structures of bimetallic clusters. J Chem Phys 124:044711
25. Kim HG, Choi SK, Lee HM (2008) New algorithm in the basin hopping Monte Carlo to find the global minimum structure of unary and binary metallic nanoclusters. J Chem Phys 128:144702
26. Wu X, Cai WS, Shao XG (2009) Optimization of bimetallic Cu–Au and Ag–Au clusters by using a modified adaptive immune optimization algorithm. J Comput Chem 30:1992–2000
27. Wu X, Wu GH, Chen YC, Qiao YY (2011) Structural optimization of Cu–Ag–Au trimetallic clusters by adaptive immune optimization algorithm. J Phys Chem A 115:13316–13323
28. Marques JMC, Pais AACC, Abreu PE (2012) On the use of big-bang method to generate low-energy structures of atomic clusters modeled with pair potentials of different ranges. J Comput Chem 33:442–452
29. Lai XJ, Xu RC, Huang WQ (2011) Geometry optimization of bimetallic clusters using an efficient heuristic method. J Chem Phys 135:164109
30. Ye T, Xu RC, Huang WQ (2011) Global optimization of binary Lennard-Jones clusters using three perturbation operators. J Chem Inf Model 51:572–577
31. Calvo F, Yurtsever E (2004) Composition-induced structural transitions in mixed rare-gas clusters. Phys Rev B 70:045423
32. Frantz DD (1996) A computational study of 13-atom Ar–Kr cluster heat capacities. J Chem Phys 105:10030–10049
33. Doye JPK, Wales DJ, Berry RS (1995) The effect of the range of the potential on the structures of clusters. J Chem Phys 103:4234–4249
34. Doye JPK, Wales DJ (2001) Polytetrahedral clusters. Phys Rev Lett 86:5719–5722
35. Doye JPK (2003) A model metal potential exhibiting polytetrahedral clusters. J Chem Phys 119:1136–1147
36. Cerbelaud M, Ferrando R, Barcaro G, Fortunelli A (2011) Optimization of chemical ordering in AgAu nanoalloys. Phys Chem Chem Phys 13:10232–10240
37. Wu X, Wu YP, Kai XM, Wu GH, Chen YC (2011) Structural optimization of Ag–Pd clusters based on different potential parameterizations. Chem Phys 390:36–41